# Comparison of Neovascular Lesion Area Measurements From Different Swept-Source OCT Angiographic Scan Patterns in Age-Related Macular Degeneration

Fang Zheng,[1,2] Qinqin Zhang,[3] Elie H. Motulsky,[1] João Rafael de Oliveira Dias,[1] Chieh-Li Chen,[3] Zhongdi Chu,[3] Andrew R. Miller,[1] William Feuer,[1] Giovanni Gregori,[1] Sophie Kubach,[4] Mary K. Durbin,[4] Ruikang K. Wang,[3] and Philip J. Rosenfeld[1]

[1]Department of Ophthalmology, Bascom Palmer Eye Institute, University of Miami Miller School of Medicine, Miami, Florida, United States
[2]Department of Ophthalmology, Tianjin Medical University General Hospital, Tianjin, China
[3]Department of Bioengineering, University of Washington, Seattle, Washington, United States
[4]Advanced Development, Carl Zeiss Meditec, Inc., Dublin, California, United States

Correspondence: Philip J. Rosenfeld, Bascom Palmer Eye Institute, 900 NW 17th Street, Miami, FL 33136, USA;
prosenfeld@miami.edu.

Submitted: June 28, 2017
Accepted: September 12, 2017

Citation: Zheng F, Zhang Q, Motulsky EH, et al. Comparison of neovascular lesion area measurements from different swept-source OCT angiographic scan patterns in age-related macular degeneration. *Invest Ophthalmol Vis Sci*. 2017;58:5098–5104. DOI: 10.1167/iovs.17-22506

**Purpose.** We compared area measurements for the same neovascular lesions imaged using swept source optical coherence tomography angiography (SS-OCTA) and enlarging scan patterns.

**Methods.** Patients with neovascular age-related macular degeneration were imaged using a 100-kHz SS-OCTA instrument (PLEX Elite 9000). The scanning protocols included the 3 × 3, 6 × 6, 9 × 9, and 12 × 12 mm fields of view. Two groups were studied. Group 1 included small lesions contained within the 3 × 3 mm scan, and Group 2 included larger lesions that were fully contained within the 6 × 6 mm scan.

**Results.** A total of 30 eyes of 26 patients were enrolled in Group 1 and 30 eyes of 25 patients were enrolled in Group 2. In Group 1, the automated mean lesion area measurements were 1.11 (SD = 0.78), 1.14 (SD = 0.80), and 1.27 (SD = 0.82) $mm^2$ for the 3 × 3, 6 × 6, and 12 × 12 mm scans, respectively (ANOVA $P < 0.001$; post hoc comparisons, $P = 0.184$, 3 × 3 vs. 6 × 6 mm; $P < 0.001$ for the other two pairs). In Group 2, the automated mean lesion area measurements were 5.43 (SD = 2.56), 5.53 (SD = 2.48), and 5.49 (SD = 2.65) $mm^2$ for the 6 × 6, 9 × 9, and 12 × 12 mm scans, respectively (ANOVA $P = 0.435$; post-hoc comparisons, $P = 0.062$, 6 × 6 vs. 9 × 9 mm; $P = 0.553$, 6 × 6 vs. 12 × 12 mm; $P = 0.654$, 9 × 9 vs. 12 × 12 mm).

**Conclusions.** The similarity in lesion area measurements across different scan patterns suggests that SS-OCTA imaging can be used to follow quantitatively the enlargement of choroidal neovascularization as the disease progresses.

Keywords: optical coherence tomography angiography, swept-source OCTA, neovascular AMD, choroidal neovascularization, quantified measurement comparison

Optical coherence tomography angiography (OCTA) is a valuable imaging strategy for diagnosing neovascular age-related macular degeneration (nvAMD).[1] In addition to the structural changes in the macula associated with neovascularization, OCTA imaging provides flow information that can identify neovascularization in the retina,[2,3] under the retina and above the retinal pigment epithelium (RPE),[4,5] and under the RPE.[6] The flow images are generated by repeating OCT B-scans at the same position and analyzing the changes between the B-scans, which usually represents the flow of erythrocytes through blood vessels.[7] The area measurements of choroidal neovascularization (CNV) imaged using OCTA have been shown to be comparable to the area measurements obtained using indocyanine green angiography (ICGA).[8] These results suggest that OCTA could be used to measure the growth of CNV and its response to therapy.

Both spectral domain (SD) and swept source (SS) OCTA instruments have been used to detect CNV.[6,9] Theoretically, SS-OCTA should be better at imaging type 1 neovascularization due to the reduced sensitivity roll-off at deeper depth and better penetration through the RPE due to the longer wavelength of the light source.[10] A recent study in our group compared the ability of SD-OCTA and SS-OCTA to detect CNV using the same segmentation strategies and artifact removal algorithm.[11] In this study, we showed that SS-OCTA imaging was better at detecting the full extent of the CNV compared to SD-OCTA imaging. A companion study published in the same issue described an automated CNV quantification algorithm that was validated against these same lesions.[12] In addition to the area of CNV, a number of potential OCTA parameters can be used to monitor the activity and progression of neovascular lesions, and these may be useful as future clinical trial endpoints.[1,13]

For routine clinical care, it is important to be able to follow the progression of lesions, especially if lesion growth could serve as the basis for retreatment or as a harbinger of exudation.

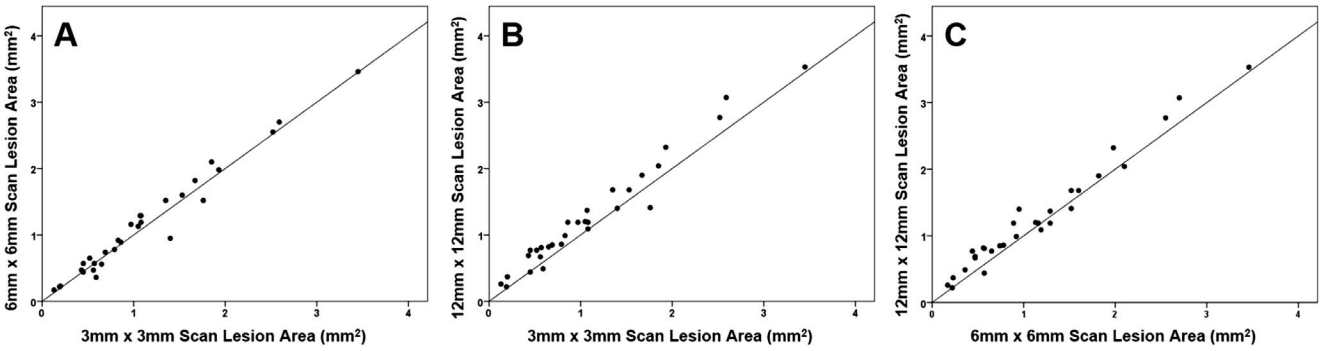


**Figure 1.** Scatter plots comparing area measurements from the small neovascular lesion group using 3 × 3, 6 × 6, and 12 × 12 mm FOV. There was a significant difference in the lesion area measurements between the different scan patterns (ANOVA, $P < 0.001$). (**A**) Comparison between 3 × 3 and 6 × 6 mm scans. No significant difference in area measurements was observed using these two scan patterns ($P = 0.184$; $r = 0.983$) (**B**) Comparison between 3 × 3 and 12 × 12 mm scans. Larger area measurements were obtained from the 12 × 12 scan patterns ($P < 0.001$; $r = 0.981$). (**C**) Comparison between 6 × 6 and 12 × 12 mm scans. Larger area measurements were obtained from the 12 × 12 mm scan patterns ($P < 0.001$; $r = 0.983$).

In clinical practice, neovascular lesions that are captured entirely within a 3 × 3 mm field of view (FOV) often enlarge to extend outside this scan area. For this reason, it is often necessary to increase the scan pattern to a 6 × 6 mm FOV. Similarly, lesions can enlarge beyond the 6 × 6 mm FOV, so it is important to increase the scan area further so as to capture the full extent of the lesion. However, it is not clear how closely lesion area measurements obtained using different scan patterns compare to each other or how useful they would be in documenting changes in the lesion area over time. One strategy to ensure that a neovascular lesion can be followed throughout its natural history is always to use the largest scan pattern available, but there is a trade-off between the size of the scans and the sampling densities (as well as the number of B-scan repetitions) that could result in loss of vascular details in smaller lesions that might become important when assessing disease progression. Another strategy is to use the smallest scan pattern to image the CNV, since this scan pattern will have the highest density of A- and B-scans; thus, providing the most reliable measurement of the neovascular lesion area. Then, as the lesion grows, the scan pattern used to image the neovascularization can be increased so that the entire lesion is contained within the scan. Therefore, it is important to know whether lesions can be measured reliably as they grow by using larger scan patterns that contain the entire lesion. To address this question, we compared the area measurements obtained when the same neovascular lesion was imaged using four different scan patterns of increasing dimensions with the same SS-OCTA instrument.

## Patients and Methods

Patients were enrolled at the Bascom Palmer Eye Institute in a prospective OCT imaging study. The institutional review board of the University of Miami Miller School of Medicine approved the study, and an informed consent to participate in the prospective OCT study was obtained from all patients. The study was performed in accordance with the tenets of the Declaration of Helsinki and compliant with the Health Insurance Portability and Accountability Act of 1996.

Patients diagnosed with CNV secondary to AMD identified previously by conventional SD-OCT structural imaging or dye-based conventional angiography were scanned on a 100-kHz SS-OCTA instrument (PLEX Elite 9000; Carl Zeiss Meditec, Dublin, CA, USA) between April 20, 2016 and April 25, 2017. This instrument has a central wavelength of 1060 nm, a bandwidth of 100 nm, an A-scan depth of 3.0 mm in tissue, a full-width at half-maximum (FWHM)[14] axial resolution of approximately 5 μm in tissue, and a lateral resolution at the retinal surface estimated at approximately 14 μm. FastTrac motion correction software was used while the images were acquired. The imaging protocols used to image the neovascular lesions included the 3 × 3, 6 × 6, 9 × 9, and 12 × 12 mm scan patterns. The 3 × 3 mm scan consisted of 300 A-scans per B-scan repeated four times at each of the 300 B-scan positions, resulting in a homogeneous sampling grid with a 10 μm spacing. The 6 × 6, 9 × 9, and 12 × 12 mm scans consisted of 500 A-scans per B-scan repeated twice at each of the 500 B-scan locations, resulting in a sampling spacing of 12, 18, and 24 μm, respectively. The neovascular lesions were divided into two groups based on size: Group 1 included CNV fully contained within the 3 × 3 mm scan area and Group 2 included CNV not contained in the 3 × 3 mm scans, but within the 6 × 6 mm scans. For Group 1, the areas of CNV were compared between the 3 × 3, 6 × 6, and 12 × 12 mm scan patterns. For Group 2, the areas of CNV were compared between the 6 × 6, 9 × 9, and 12 × 12 mm scan patterns. All OCTA images of a given patient were acquired in a single session by an experienced operator. The exclusionary criteria included a signal strength lower than 7/10, presence of excessive motion artifacts, and unfocused scans.

Visualization of the retinal and choroidal vasculature from the volumetric datasets was achieved using a method known as optical microangiography, based on the complex OCT signal ($OMAG^C$).[7,15] The $OMAG^C$ algorithm incorporates variations in the intensity and phase information between sequential B-scans at the same position to generate the flow information. The same segmentation and image processing strategies were applied to all scanning protocols. The segmentation boundaries for the slab used in this study extended from the outer boundary of the outer plexiform layer (OPL) to 8 μm beneath Bruch's membrane. This slab, referred to as the outer retina to choriocapillaris (ORCC) slab, should contain types 1 and 2 CNV.[6] Removal of the retinal projection artifacts from the overlying retinal vasculature onto the ORCC slab was performed as described previously.[16,17] A validated automated algorithm was used to measure the area of the CNV in the en face artifact-free ORCC images.[12] As described previously, the contrast of the artifact-free ORCC angiogram was enhanced through an adaptive thresholding method. The differences of sampling spaces in different scanning protocols resulted in different contrast-to-noise ratios (CNRs) with higher CNR found in the 3 × 3 and 6 × 6 mm scans and lower CNR found

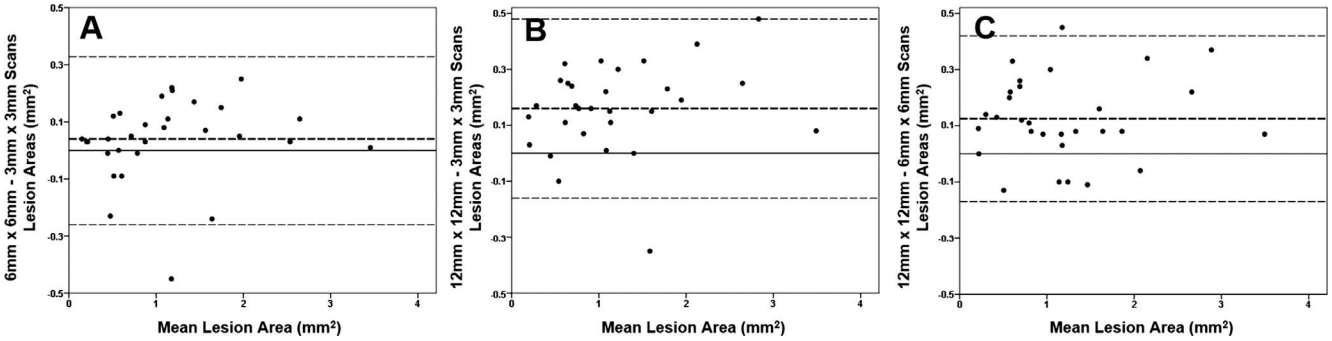


**Figure 2.** Bland-Altman plots showing the difference in area measurements for the small neovascular lesion group using 3 × 3, 6 × 6, and 12 × 12 mm fields of view. The *bold dashed line* represents the mean difference and the *top* and *bottom dashed lines* indicate the 95% tolerance limits. (**A**) Plots of 3 × 3 and 6 × 6 mm scan patterns with a mean difference of 0.04 mm$^2$ ($P = 0.184$). (**B**) Plots of 3 × 3 and 12 × 12 mm scan patterns with a mean difference of 0.16 mm$^2$ ($P < 0.001$). (**C**) Plots of 6 × 6 and 12 × 12 mm scan patterns with a mean difference of 0.13 mm$^2$ ($P < 0.001$).

in 9 × 9 and 12 × 12 mm scans.[11] A region of interest (ROI) was selected automatically within the image and the boundary outline for the CNV was detected through mathematical morphologic analysis. We used a 3 × 3 ROI in Group 1 and a 6 × 6 ROI in Group 2 for the area measurements of CNV to exclude the noise in the larger scans, especially the 12 × 12 mm scans.

Lesion areas obtained using different SS-OCTA scan patterns were compared. Pearson's $r$ was used to summarize the strength of the correlations. The means of lesion sizes measured with different scan patterns were compared with repeated measures ANOVA followed by post hoc least significant difference (LSD) tests. The differences between lesion sizes made with different scan patterns also were assessed with Bland-Altman analyses. Statistical analysis was performed with IBM SPSS Statistics for Windows, Version 22.0 (IBM Corporation, Armonk, NY, USA).

## Results

A total of 30 eyes of 26 patients were enrolled in Group 1 and 30 eyes of 25 patients were enrolled in Group 2. Women comprised 18 (69.2%) of 26 patients in Group 1 and 17 (68%) of 25 patients in Group 2. Mean patient age was 78.4 years (range, 51–95 years) in Group 1 and 79.1 years (range, 63–89 years) in Group 2. At the time of imaging, 52 of 60 eyes had received prior intravitreal therapy with VEGF inhibitors, three eyes received an injection on the day of imaging due to new onset exudation, and five eyes had subclinical CNV without exudation and were being observed.

In Group 1, the mean area measurements for the 3 × 3, 6 × 6, and 12 × 12 mm scans were 1.11 (SD = 0.78; range, 0.13–3.45), 1.14 (SD = 0.80; range, 0.17–3.46), and 1.27 (SD = 0.82; range, 0.26–3.53) mm$^2$, respectively. ANOVA showed a significant difference in area measurements between 3 × 3, 6 × 6, and 12 × 12 mm scans ($P < 0.001$). Post hoc LSD

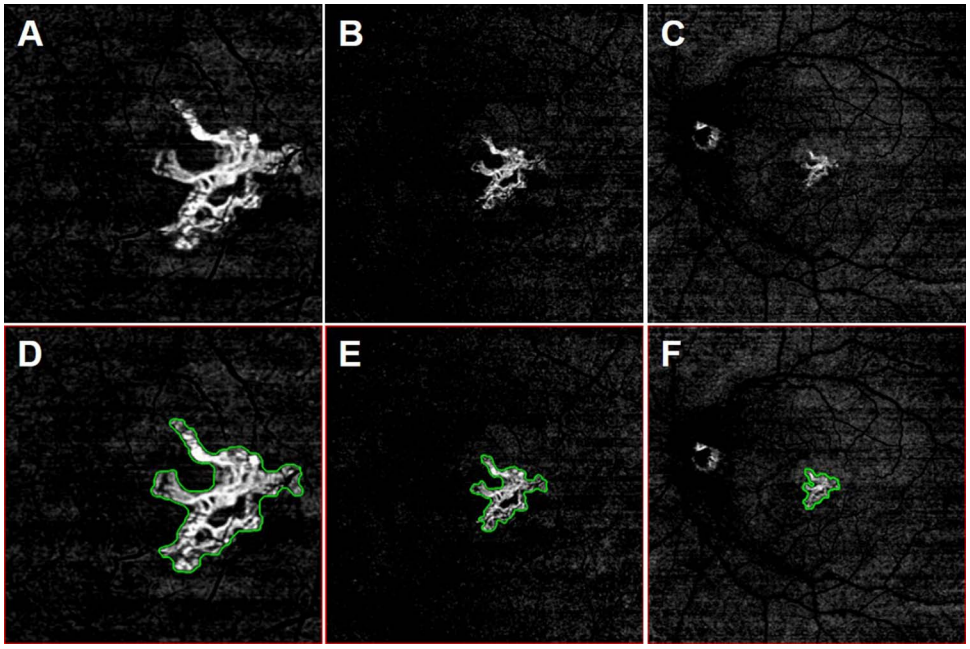


**Figure 3.** En face flow images from the left eye of a 74 year-old woman with CNV. The CNV was identified from a slab with segmentation boundaries that extended from the ORCC. (**A**) 3 × 3 mm ORCC image. (**B**) 6 × 6 mm ORCC image. (**C**) 12 × 12 mm ORCC image. (**D**) 3 × 3 mm ORCC image with the CNV outlined (area = 0.86 mm$^2$). (**E**) 6 × 6 mm ORCC image with the CNV outlined (area = 0.89 mm$^2$). (**F**) 12 × 12 mm ORCC image with the CNV outlined (area = 1.19 mm$^2$).

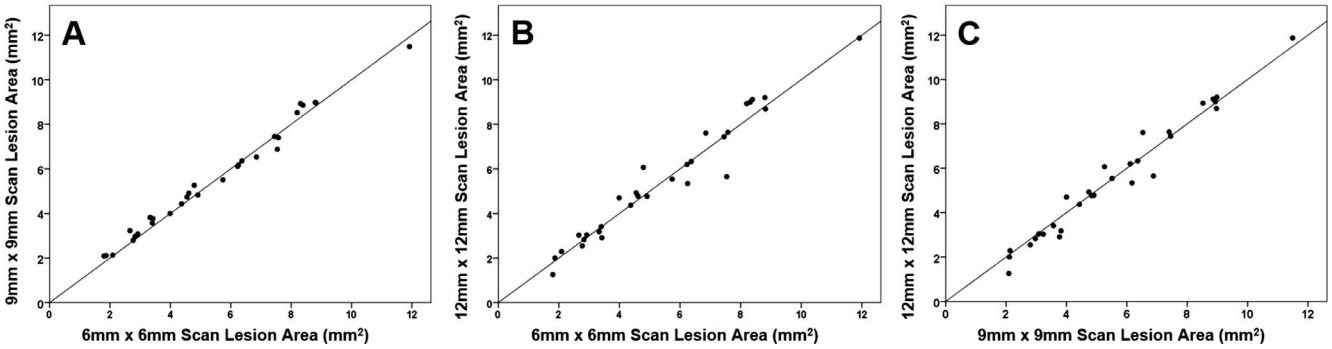


FIGURE 4. Scatter plots comparing area measurements from the larger neovascular lesion group using 6 × 6, 9 × 9, and 12 × 12 mm FOV. There were no differences in the lesion area measurements between all the different scan patterns (ANOVA $P = 0.435$). (**A**) Comparison between 6 × 6 and 9 × 9 mm scans. The correlation coefficient was $r = 0.994$. (**B**) Comparison between 6 × 6 and 12 × 12 mm scans. The correlation coefficient was $r = 0.976$. (**C**) Comparison between 9 × 9 and 12 × 12 mm scans. The correlation coefficient was $r = 0.984$.

comparisons demonstrated that the area measurements obtained from the 12 × 12 mm scan pattern were significantly larger than those of the other two scans ($P < 0.001$), while there was no significant difference in the area measurements obtained from the 3 × 3 and 6 × 6 mm scans ($P = 0.184$). Figure 1A shows the area measurements from the 30 eyes imaged using the 3 × 3 and 6 × 6 mm scan patterns ($r = 0.983$). Differences between areas measurements using these two scan patterns were not correlated with the lesion sizes (Fig. 2A). When the 12 × 12 mm scan pattern was used on these smaller lesions in Group 1, the area measurements tended to be larger than those obtained with the 3 × 3 and 6 × 6 mm scans with 0.16 and 0.13 mm$^2$ mean difference, respectively, as shown by the greater proportion of data points above the line of unity in Figures 1B and 1C. The Bland-Altman plots further helped visualize these findings, showing mean differences that were significantly larger than zero ($P < 0.001$; Figs. 2B, 2C). Figure 3 is an example of a neovascular lesion with similar area measurements with the 3 × 3 and 6 × 6 mm scans, but a larger area measurement with the 12 × 12 mm scan.

In Group 2, the mean area measurements were 5.43 (SD = 2.56; range, 1.80–11.92), 5.53 (SD = 2.48; range, 2.09–11.49), and 5.49 (SD = 2.65; range, 1.26–11.87) mm$^2$ for the 6 × 6, 9 × 9, and 12 × 12 mm scans, respectively. Overall, in Group 2 there were no differences in the lesion area measurements between the different scan patterns (ANOVA $P = 0.435$). Figures 4 and 5 show the scatter plots and Bland-Altman plots of the comparisons between the 6 × 6, 9 × 9, and 12 × 12 mm scans for the 30 eyes in Group 2. The correlations between the area measurements from the three scan patterns were excellent ($r > 0.95$; $P < 0.001$ for all comparisons). The mean difference between the lesion area measurements was 0.10 mm$^2$ on the 9 × 9 and 6 × 6 mm scans (SD = 0.30; $P = 0.062$), 0.06 mm$^2$ on the 12 × 12 and 6 × 6 mm scans (SD = 0.58, P = 0.553); and –0.04 mm$^2$ (SD = 0.50; $P = 0.654$) on the 12 × 12 and 9 × 9 mm scans. Figure 6 shows an example with good agreement between scans. Figure 7 shows slightly different area measurements obtained using the different scan patterns.

## DISCUSSION

Area measurements of CNV can be influenced by the sampling density of A- and B-scans and by the number of B-scan repeats, which can vary between different scan patterns and affect image quality as described previously.[12] Higher scan densities and more B-scan repeats at the same position can result in a higher CNR and, therefore, a better image quality. The 3 × 3 mm scans have the highest densities and repeated number of B-scans. However, we found that neovascular lesions in clinical practice were frequently larger than the 3 × 3 mm scan pattern and not fully contained within the scan. Therefore, it is not practical to image and follow all CNVs using a single 3 × 3 mm scan centered on the fovea. The larger scan patterns, which include the 6 × 6, 9 × 9, and 12 × 12 mm scans, all consisted of 500 A-scans per B-scan with two repeated B-scans at each position. Consequently, as the FOV increases, the spacing between A- and B-scans increases, which could potentially compromise the ability to image small vascular details reliably. However, based on our results, this only becomes a significant

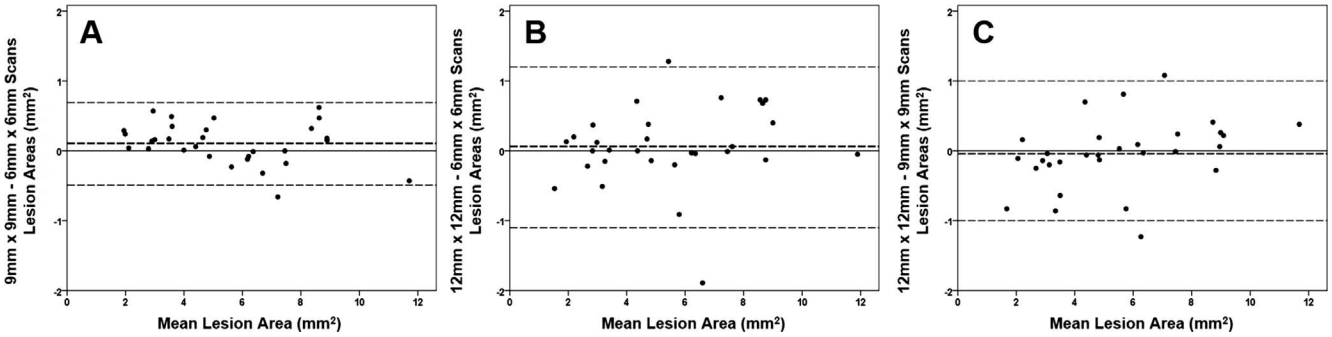


FIGURE 5. Bland-Altman plots showing the difference in area measurements for the larger neovascular lesion group using 6 × 6, 9 × 9, and 12 × 12 mm FOV. The *bold dashed line* represents the mean difference and the *top* and *bottom dashed lines* indicate the 95% tolerance limits. (**A**) Plots of 6 × 6 and 9 × 9 mm scan patterns with a mean difference of 0.10 mm$^2$ ($P = 0.062$). (**B**) Plots of 6 × 6 and 12 × 12 mm scan patterns with a mean difference of 0.06 mm$^2$ ($P = 0.553$). (**C**) Plots of 6 × 6 and 12 × 12 mm scan patterns with a mean difference of –0.04 mm$^2$ ($P = 0.654$).

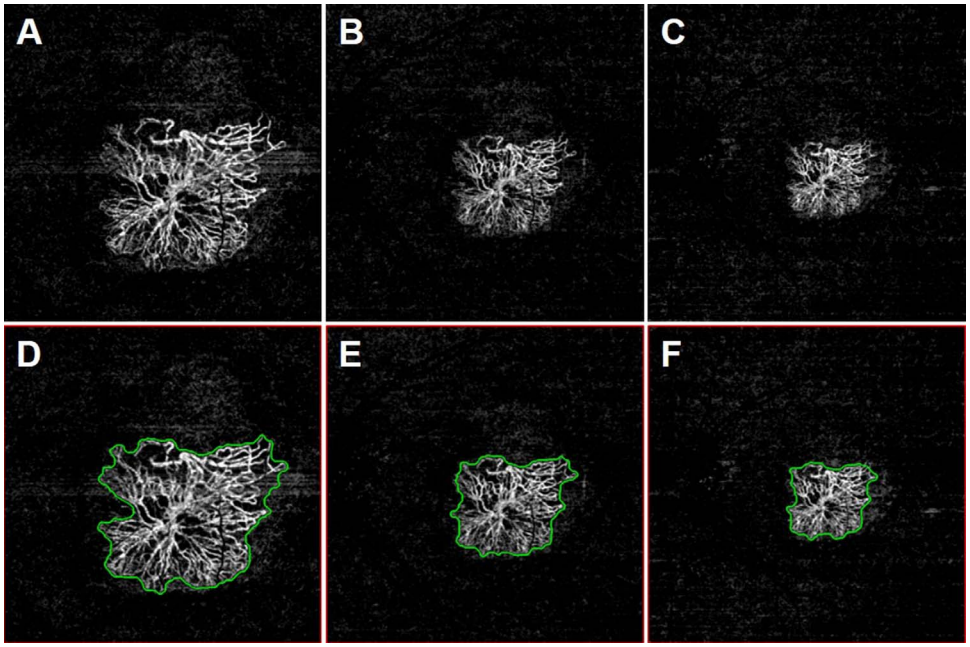


**Figure 6.** En face flow images from the left eye of an 82-year-old woman with CNV. The CNV was identified from a slab with segmentation boundaries that extended from the ORCC. There was good agreement between the 6 × 6, 9 × 9, and 12 × 12 mm scan patterns. (**A**) 6 × 6 mm ORCC image. (**B**) 9 × 9 mm ORCC image. (**C**) 12 × 12 mm ORCC image. (**D**) 6 × 6 mm ORCC image with the CNV outlined (area = 7.45 $mm^2$). (**E**) 9 × 9 mm ORCC image with the CNV outlined (area = 7.45 $mm^2$). (**F**) 12 × 12 mm ORCC image with the CNV outlined (area = 7.44 $mm^2$).

issue when the smaller lesions are imaged using the 12 × 12 mm scan pattern. We showed that the 6 × 6 mm scans yielded similar area measurements compared to the 3 × 3 mm scans, which was reassuring given the fact that these smaller lesions in Group 1 often grow beyond the 3 × 3 mm FOV. In addition, we showed that the larger lesions in Group 2 could be imaged with increasingly larger scan patterns, and the area measurements obtained with the 6 × 6 mm scans were comparable to the area measurements obtained using 9 × 9 and 12 × 12 mm scans. Thus, it stands to reason that the best initial scan to assess CNV is the 6 × 6 mm scan. If the identified lesion is smaller and greater vascular detail is desired, then the 3 × 3 mm scan should be performed to achieve the best image quality. If the lesion is larger than the 6 × 6 mm scan, then the

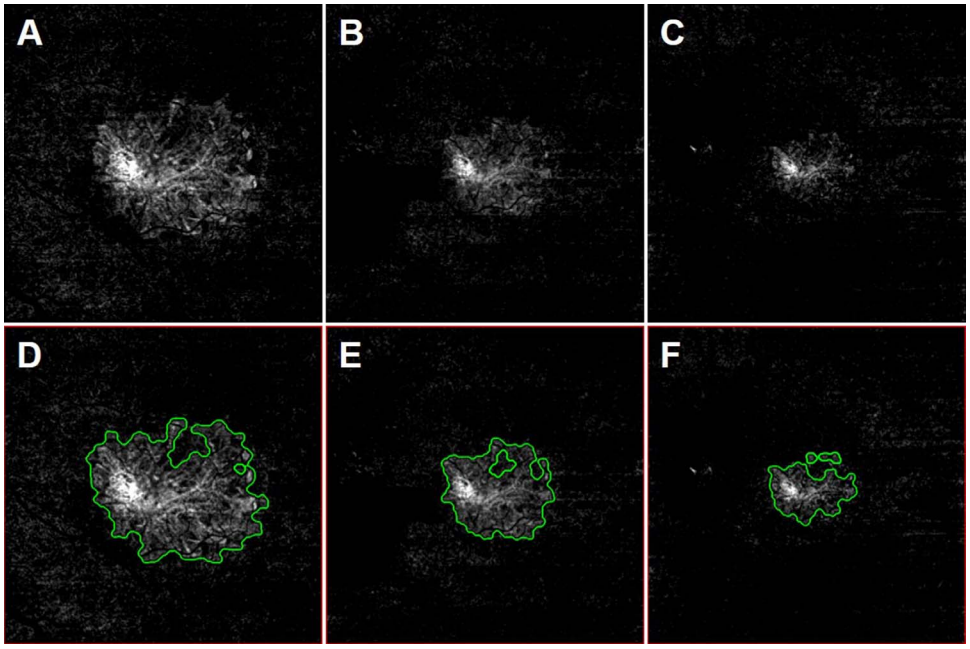


**Figure 7.** En face flow images from the left eye of a 66-year-old man with CNV. The CNV was identified from a slab that extended from the ORCC. There was slightly difference between area measurements obtained using the 6 × 6, 9 × 9, and 12 × 12 mm scan patterns. (**A**) 6 × 6 mm ORCC image. (**B**) 9 × 9 mm ORCC image. (**C**) 12 × 12 mm ORCC image. (**D**) 6 × 6 mm ORCC image with the CNV outlined (area = 6.25 $mm^2$). (**E**) 9 × 9 mm ORCC image with the CNV outlined (area = 6.17 $mm^2$). (**F**) 12 × 12 mm ORCC image with the CNV outlined (area = 5.34 $mm^2$).

next larger scan pattern should be used to visualize the entire lesion while obtaining the best image quality for that particular lesion.

One of the reasons why the Group 1 smaller lesions had larger area measurements in the 12 × 12 mm scans was due to the loss of image quality from the increased spacing between A- and B-scans. This resulted in a smoothing of the lesions' borders, which can be readily appreciated when comparing the images to those acquired using the 3 × 3 mm scan pattern. The loss of boundary details resulted in the quantification algorithm calculating larger area measurements (Fig. 3). Another possibility is that there could be a loss in the sensitivity of flow detection when larger scan patterns were used due to the decreased number of B-scan repeats. In this situation, a smaller area measurement might be obtained as shown in Figure 7.

Limitations of this study included a small sample size and the use of segmentation and image processing strategies[6,12,16,17] that were not yet commercially available at the time this study was performed. To be used in the study, we required that all scans had to have a signal strength of at least 7/10 and that poor-quality scans were excluded from the analyses so that the quantitative comparisons between different scan patterns could be performed. However, many of the images that were excluded would have sufficed in the routine clinical care of patients where the goal of imaging is to determine the presence or absence of CNV. In addition, we only examined small lesions fully contained within the 3 × 3 mm scans (Group 1) and larger lesions contained within the 6 × 6 mm scans (Group 2). We decided not to study even larger lesions, since the vast majority of neovascular lesions in clinical practice are contained within the 6 × 6 mm scan pattern. It also stands to reason that if the area measurements from the 6 × 6 mm scans were comparable to the area measurements from the 9 × 9 and 12 × 12 mm scans, then larger lesions contained within the 9 × 9 mm scans should be comparable to the 12 × 12 mm scans.

In conclusion, we found no difference between 3 × 3 and 6 × 6 mm scans for small lesions and there were no differences between 6 × 6, 9 × 9, and 12 × 12 mm scans for larger lesions. We recommend that the 6 × 6 mm scans should be used as the first scan pattern of choice when imaging patients with CNV. Once the CNV is identified, the 3 × 3 mm scan pattern can be used for smaller lesions to optimize visualization of the neovascular details, and the 9 × 9 or 12 × 12 mm scan patterns can be used to image CNV that exceeds the 6 × 6 mm FOV. Larger scan patterns also are useful for identifying satellite neovascular lesions that may not be contiguous with main area of neovascularization. To date, the most common quantitative OCT parameter used in clinical trials has been the measurement of OCT central retinal thickness.[18–20] However, OCTA is gaining popularity as a way to follow neovascular lesions qualitatively in clinical practice,[13,21,22] and we are ready to recommend the use of SS-OCTA to follow neovascular lesions quantitatively in clinical trials.

## Acknowledgments

Supported by grants from Carl Zeiss Meditec, Inc. (Dublin, CA, USA), the National Eye Institute (R01EY024158), an unrestricted grant from the Research to Prevent Blindness, Inc., New York, NY, USA, and the National Eye Institute Center Core Grant (P30EY014801) to the Department of Ophthalmology, University of Miami Miller School of Medicine.

Disclosure: **F. Zheng**, None; **Q. Zhang**, None; **E.H. Motulsky**, None; **J.R. de Oliveira Dias**, None; **C.-L. Chen**, None; **Z. Chu**, None; **A.R. Miller**, None; **W. Feuer**, None; **G. Gregori**, Carl Zeiss Meditec (F), P; **S. Kubach**, Carl Zeiss Meditec (E); **M.K. Durbin**, Carl Zeiss Meditec (E); **R.K. Wang**, Carl Zeiss Meditec (F), Tasso, Inc. (F), Insight Photonic Solutions (C), Westface Medical (C), Kowa (C), P; **P.J. Rosenfeld**, Acucela (C, F), Alcon (C), Apellis (F, I), Boehringer-Ingelheim (C), Carl Zeiss Meditec (C, F), Cell Cure Neurosciences (C), Chengdu Kanghong Biotech (C), Digisight (I), F. Hoffmann-La Roche Ltd. (C), Genentech (C, F), GlaxoSmithKline (F), Astellas Institute for Regenerative Medicine (F), Healios K.K. (C), Hemera Biosciences (C), Isarna Pharmaceuticals (C), MacRegen Inc. (C), Ocudyne (C, I), Ocunexus Therapeutics (C), Tyrogenex (C, F), Unity Biotechnology (C)

## References

1. Cole ED, Ferrara D, Novais EA, Louzada RN, Waheed NK. Clinical trial endpoints for optical coherence tomography angiography in neovascular age-related macular degeneration. *Retina*. 2016;36(suppl 1):S83–S92.
2. Kuehlewein L, Dansingani KK, de Carlo TE, et al. Optical coherence tomography angiography of type 3 neovascularization secondary to age-related macular degeneration. *Retina*. 2015;35:2229–2235.
3. Miere A, Querques G, Semoun O, El Ameen A, Capuano V, Souied EH. Optical coherence tomography angiography in early type 3 neovascularization. *Retina*. 2015;35:2236–2241.
4. Parravano M, Querques L, Scarinci F, et al. Optical coherence tomography angiography in treated type 2 neovascularization undergoing monthly anti-VEGF treatment. *Acta Ophthalmol*. 2016;95:e425–e426.
5. Souied EH, El Ameen A, Semoun O, Miere A, Querques G, Cohen SY. Optical coherence tomography angiography of type 2 neovascularization in age-related macular degeneration. *Dev Ophthalmol*. 2016;56:52–56.
6. Roisman L, Zhang Q, Wang RK, et al. Optical coherence tomography angiography of asymptomatic neovascularization in intermediate age-related macular degeneration. *Ophthalmology*. 2016;123:1309–1319.
7. Huang Y, Zhang Q, Thorell MR, et al. Swept-source OCT angiography of the retinal vasculature using intensity differentiation-based optical microangiography algorithms. *Ophthal Surg Lasers Imag Retina*. 2014;45:382–389.
8. Costanzo E, Miere A, Querques G, Capuano V, Jung C, Souied EH. Type 1 Choroidal neovascularization lesion size: indocyanine green angiography versus optical coherence tomography angiography. *Invest Ophthalmol Vis Sci*. 2016;57:307–313.
9. Iafe NA, Phasukkijwatana N, Sarraf D. Optical coherence tomography angiography of type 1 neovascularization in age-related macular degeneration. *Dev Ophthalmol*. 2016;56:45–51.
10. Potsaid B, Baumann B, Huang D, et al. Ultrahigh speed 1050nm swept source/Fourier domain OCT retinal and anterior segment imaging at 100,000 to 400,000 axial scans per second. *Opt Exp*. 2010;18:20029–20048.
11. Miller AR, Roisman L, Zhang Q, et al. Comparison between spectral-domain and swept-source optical coherence tomography angiographic imaging of choroidal neovascularization. *Invest Ophthalmol Vis Sci*. 2017;58:1499–1505.
12. Zhang Q, Chen CL, Chu Z, et al. Automated quantitation of choroidal neovascularization: a comparison study between spectral-domain and swept-source OCT angiograms. *Invest Ophthalmol Vis Sci*. 2017;58:1506–1513.
13. Jia Y, Bailey ST, Wilson DJ, et al. Quantitative optical coherence tomography angiography of choroidal neovascularization in age-related macular degeneration. *Ophthalmology*. 2014;121:1435–1444.
14. Tomlins PH, Wang RK. Theory, developments and applications of optical coherence tomography. *J Phys D*. 2005;38:2519–2535.

15. Wang RK, An L, Francis P, Wilson DJ. Depth-resolved imaging of capillary networks in retina and choroid using ultrahigh sensitive optical microangiography. *Opt Lett*. 2010;35:1467–1469.
16. Zhang A, Zhang Q, Wang RK. Minimizing projection artifacts for accurate presentation of choroidal neovascularization in OCT micro-angiography. *Biomed Opt Exp*. 2015;6:4130–4143.
17. Zhang Q, Zhang A, Lee CS, et al. Projection artifact removal improves visualization and quantitation of macular neovascularization imaged by optical coherence tomography angiography. *Ophthalmol Retina*. 2017;1:124–136.
18. Fung AE, Lalwani GA, Rosenfeld PJ, et al. An optical coherence tomography-guided, variable dosing regimen with intravitreal ranibizumab (Lucentis) for neovascular age-related macular degeneration. *Am J Ophthalmol*. 2007;143:566–583.
19. Lalwani GA, Rosenfeld PJ, Fung AE, et al. A variable-dosing regimen with intravitreal ranibizumab for neovascular age-related macular degeneration: year 2 of the PrONTO Study. *Am J Ophthalmol*. 2009;148:43–58 e41.
20. Maguire MG, Martin DF, Ying GS, et al.; for the Comparison of Age-Related Macular Degeneration Treatments Trials (CATT) Research Group. Five-year outcomes with anti-vascular endothelial growth factor treatment of neovascular age-related macular degeneration: the comparison of age-related macular degeneration treatments trials. *Ophthalmology*. 2016;123:1751–1761.
21. Lumbroso B, Rispoli M, Savastano MC. Longitudinal optical coherence tomography-angiography study of type 2 naive choroidal neovascularization early response after treatment. *Retina*. 2015;35:2242–2251.
22. Huang D, Jia Y, Rispoli M, Tan O, Lumbroso B. Optical coherence tomography angiography of time course of choroidal neovascularization in response to anti-angiogenic treatment. *Retina*. 2015;35:2260–2264.

Investigative Ophthalmology & Visual Science